Communication

Gold Nanostar-Based Sensitive Catechol Plasmonic Colorimetric Sensing Platform with Ultra-Wide Detection Range

Huafeng Wang [1], Ting Fang [1], Hua Liu [1], Tianxiang Wei [2,*] and Zhihui Dai [1,3,*]

1 Jiangsu Collaborative Innovation Center of Biomedical Functional Materials, Jiangsu Key Laboratory of Biofunctional Materials, School of Chemistry and Materials Science, Nanjing Normal University, Nanjing 210023, China
2 School of Environment, Nanjing Normal University, Nanjing 210023, China
3 School of Chemistry and Molecular Engineering, Nanjing Tech University, Nanjing 211816, China
* Correspondence: weitian_xiang@126.com (T.W.); daizhihuii@njnu.edu.cn (Z.D.)

Abstract: High sensitivity and a wide detection range are always the pursuit of sensor design. In this work, gold nanostars (Au NSs) featuring the shape of sea urchins with an absorption peak at the near infrared region (822 nm) were prepared. We proposed a Au NSs-based plasmonic colorimetric sensing platform for ultrasensitive catechol (CC) detection with a wide detection range from 3.33 nM to 107 μM and a limit of detection (LOD) at 1 nM. The target analyte, CC, was used to reduce silver ions (Ag^+) to form silver (Ag) coating on the surface of Au NSs, which caused a blue-shift in the localized surface plasmon resonance (LSPR) of Au NSs. With the gradual increase in CC concentration, the Ag coating on the surface was gradually nucleated, and the LSPR blue-shift carried on. This strategy yields a wide LSPR shift by as much as 276 nm for plasmonic effects, enabling an ultra-wide range and the ultrasensitive detection of CC. This work will facilitate the research of target-mediated LSPR sensors and their wide application in environmental monitoring, food safety, and disease diagnosis.

Keywords: gold nanostar; colorimetric; catechol; localized surface plasmon resonance; blue-shift

1. Introduction

Catechol (CC) is an essential chemical intermediate extensively used in the production of pharmaceuticals, antioxidants, and cosmetics [1]. However, CC is highly susceptible to soil and groundwater contamination due to its low degradation rate. CC has been classified into the II B carcinogen list and environmental pollutants in many countries because of its high toxicity and hard degradation in the ecological environment, threatening human life and health [2]. Therefore, there is an urgent demand to address the sensitive and convenient detection of CC in the field of environmental monitoring. To solve this problem, several methods have been developed to enable the efficient and accurate detection of CC, including high performance liquid chromatography [3], surface-enhanced Raman spectroscopy [4], electrochemistry [5–7], and fluorescence spectroscopy [8]. Although these approaches have many benefits of better accuracy and high sensitivity, they are still plagued by expensive and complicated instruments, time-consuming modification processes, and weak anti-interference ability. In contrast, visible (vis) absorption spectrometry has attracted widespread attention for its ease of operation, high accuracy, strong anti-interference, and the convenience of visual ability.

Recently, noble metal nanomaterials have attracted extensive attention due to their unique optical properties [9–18]. The enhanced localized surface plasmon resonance (LSPR) of noble metal nanoparticles (NPs) makes them effective absorbers and scatterers, promoting their applications in biochemical sensing and imaging [19–23]. Since their SPR absorption is highly sensitive to the compositions, sizes, shapes, and surrounding microenvironment [24], gold (Au) or silver (Ag) NPs-based colorimetric methods have been

reported for the sensitive detection of multiple targets including small molecules, antigens, and nucleic acids [25–29]. Among them, Au NPs have been extensively reported for LSPR-based colorimetric detection. For example, spherical Au NPs have been widely employed to construct numerous colorimetric sensors for detecting deoxyribonucleic acid (DNA) [30,31], protein [32–34], and heavy metal ions [35–37]. For the detection of phenols, LSPR colorimetric sensors with spherical or rod-shaped Au NPs have also been investigated [23,38]. Choi et al. observed different plasma effects by reducing silver ions (Ag$^+$) in Au NPs suspensions by three isomers of benzenediol [39]. Although these methods have made progress in various aspects, there are still common shortcomings owing to the limited maximum absorption wavelength of Au NPs at around 520 nm, such as limited detection range and low sensitivity [40].

Gold nanostars (Au NSs) possess multi-branched nanostructures with many protruding arms bearing sharp tips, which enables the local field intensity near the tips significantly higher than the incident light, presenting a broad potential for plasmon-enhanced spectroscopy [41–43]. In this work, based on Au NSs featuring the shape of sea urchins and near-infrared (NIR) absorption peaks higher than 800 nm, a target-mediated plasmonic effect change strategy was subtly constructed for CC detection (Scheme 1). In the colorimetric system, less CC can reduce Ag$^+$ to realize the rapid epitaxial growth of Ag nanocrystal coating on the surface of Au NSs, which yields blue-shifts of the LSPR and color changes. As the concentration of CC gradually increases, the Ag coating on the surface is gradually nucleated, and the LSPR shift is gradually increased. The color eventually changes to yellow. This strategy enables a wide range shift of 276 nm for the plasmonic effect with wide-range detection of CC from 3.33 nM to 107 μM, and provides a method for the sensitive detection of CC, which can also provide reference for other plasmonic colorimetric sensing platforms to achieve high sensitivity and a wide detection range.
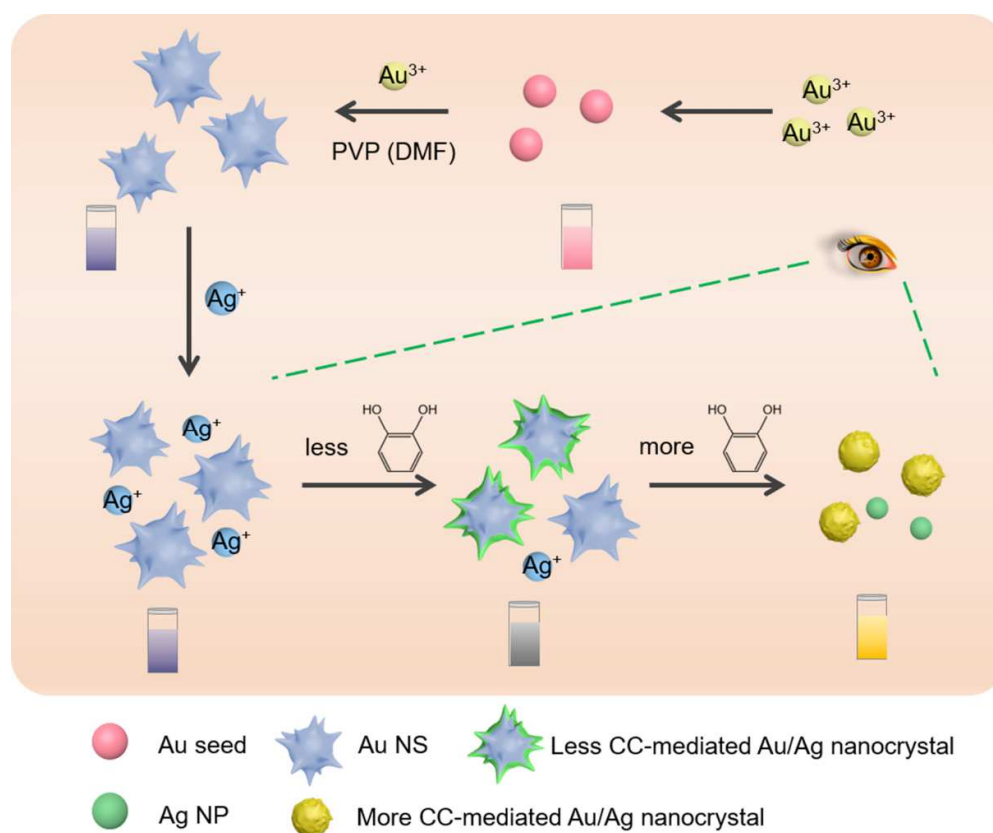
Scheme 1. Schematic illustration of the plasmonic colorimetric sensor for the detection of CC.

2. Materials and Methods

2.1. Materials and Apparatus

Gold(III) chloride trihydrate ($HAuCl_4 \cdot 3H_2O$), sodium citrate, polyvinylpyrrolidone (PVP), N,N-dimethylformamide (DMF), CC, *m*-cresol, *p*-cresol, bisphenol A, silver nitrate ($AgNO_3$), and ammonia (NH_4OH) were purchased from Sigma-Aldrich. A filter device was provided by Merck Millipore (Burlington, MA, USA). Deionized (DI) water from Millipore purification system was used for all experiments. UV-vis absorption spectra were recorded by Cary 60 UV spectrophotometer (Agilent, Santa Clara, CA, USA). Scanning transmission electron microscopy with energy dispersive X-ray spectra (STEM-EDS) was characterized using JEOL JEM-2100F operated at an accelerating voltage of 200 kV. Transmission electron microscope (TEM) images were recorded using Hitachi H-7650 at the accelerating voltage of 80 kV.

2.2. Synthesis of PVP-Coated Au Seeds

According to the previous reports with slight changes [44], PVP-coated Au seeds were prepared with the following procedures: 225 µL of 100 mM $HAuCl_4$ water solution was added in 90 mL ultrapure water, heated to boiling, and stirred vigorously. Then, 2.7 mL of 1% sodium citrate was quickly mixed with 90 mL of $HAuCl_4$ boiling solution (0.27 mM) under vigorous stirring and kept boiling for 10 min to obtain a wine-red solution. Then 7.5 mL of the obtained solution and 6.5 mL of 2.56 mM PVP aqueous solution were mixed and stirred for 1 h in the dark. Subsequently, the resulting reaction solution was centrifuged at 11,000 rpm for 15 min to remove the unattached PVP. Finally, the synthesized PVP-coated Au seeds precipitates were re-dissolved in 1 mL of ethanol.

2.3. Preparation of Au NSs

Au NSs were prepared according to previous reported with some modifications [10]. Briefly, 41 µL of 100 mM $HAuCl_4$ was mixed with 15 mL of 10 mM PVP in the DMF solution, then quickly added into 100 µL of PVP-coated Au seeds, and further stirred at room temperature. The solution changed from pink to colorless and finally to dark blue in 15 min, demonstrating the synthesis of Au NSs in solution.

2.4. Construction of Au NSs-Based CC Plasmonic Colorimetric Sensing Platform

The Au NSs solution was centrifuged and dispersed in 10 mL of 100 mM $NaHCO_3$ buffer (pH 9). Then 1 mL of 50% glutaraldehyde was added and stirred for 3 h. The mixture was redispersed in 10 mL of 100 mM $NaHCO_3$ buffer after washing and centrifugation. 0.1 mM silver nitrate, 40 mM ammonia, and appropriate concentrations of CC solution were added sequentially and reacted for 2 h. Finally, UV-vis absorption spectra were measured by spectrophotometer.

2.5. Application of the Colorimetric Sensor in Real Samples

Tap water and industrial wastewater were selected as the real samples to evaluate the capability. The industrial wastewater was filtered through a 0.22 µm membrane and diluted 1000 times. The standard addition method was employed to determine CC in tap water and industrial wastewater.

3. Results and Discussion

3.1. Characteristics of Au Seeds, Au NSs, and Au/Ag Nanocrystal

The prepared Au seeds, Au NSs, and CC-reduced Au/Ag nanocrystals were characterized by UV-vis absorption spectroscopy and TEM. As shown in Figure 1A, the Au seeds are well dispersed, nearly spherical, and uniform in size with an average particle size of 17.9 nm. Au NSs were synthesized using a typical and efficient method for seed-mediated growth. The Au seeds were used for the growth of the nucleus, and Au^{3+} was reduced with the reducing agent PVP [45]. In the effect of PVP, the Au seed is a growth point, and multiple branched angles are formed on the surface to form Au nanoarms. Having long

and sharp branches is one of the most characteristic features for star-shaped structures [46]. As shown in the TEM image of Figure 1B, the sea urchin-like Au NSs were successfully prepared with uniform particle dispersion. Subsequently, the corresponding UV absorption spectra of various samples were performed (Figure 1C). The absorption peak of Au seed was 521 nm (a), while Au NS was shifted to 822 nm, which proved that the synthesized Au NSs possess NIR absorption. Interestingly, when a trace amount of CC was introduced to the system, the surface of Au NSs became blurred, and even several circular low-contrast Ag nanocrystals could be observed (Figure 1D). The color of Au seeds and Au NSs were pictured in Figure 1E, which was consistent with the results previously reported [39]. The changed color of CC-reduced Au/Ag nanocrystals preliminarily illustrated the feasibility of colorimetric sensing for CC detection.
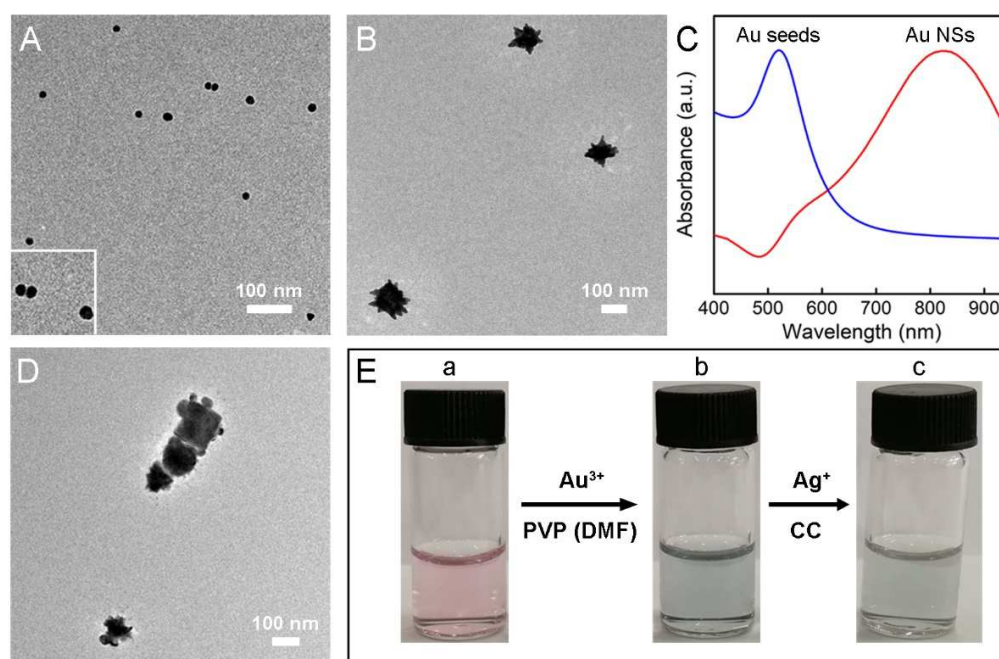

Figure 1. (**A**) TEM image of Au seeds. The insert was the partially enlarged TEM image of Au seeds. (**B**) TEM image of Au NSs. (**C**) UV-vis absorption spectra of Au seeds and Au NSs. (**D**) TEM image of 26.7 μM CC-mediated reduction of Ag^+ on the Au NSs. (**E**) Photographs of (**a**) Au seeds, (**b**) Au NSs, and (**c**) 5.33 μM CC-mediated reduction of Ag^+ on the Au NSs.

3.2. Feasibility of the Au NSs-Based Ultrasensitive CC Plasmonic Colorimetric Sensing

To verify the feasibility of the constructed strategy, the effects of different concentrations of CC on the Au NSs reaction system were investigated by STEM-EDS and UV-vis spectroscopy. STEM-EDS elemental mapping images exhibited the spatial arrangement of virous elements. As shown in Figure 2A, when adding 14.0 μM CC into the Au NSs system, Ag^+ were reduced, and the epitaxial growth of Ag nanocrystal thin coating on the surface of Au NSs could be observed. A higher concentration of CC (40.0 μM) induced thicker Ag coating and small amounts of individual Ag NPs (Figure 2B). The STEM-EDS results demonstrated the changing process of Ag nanocrystal nucleation, as well as the evolution of Au NSs from multi-armed branching to a rough surface and finally to being relatively smooth with the increase in CC concentration. This reflected the fact that Ag^+ reduced to the Ag shell by CC and then gradually nucleated and grew into individual Ag NPs. The EDS spectrum further proved the fact that the content of Ag increased with the increment of CC concentration (Figure 2C,D). The UV-vis absorption spectra in Figure 2E presented a gradual plasmonic blue-shift by 115 nm and 228 nm, respectively, proving the feasibility that the reduction of Ag^+ by CC could trigger the plasma resonance effects. It could be obviously observed that a new wide absorption band at 342–482 nm appeared with the increment of CC concentration (curve b in Figure 2E), which may be owing to

the formation of Ag NPs [39,47]. To further investigate the reaction process in this Au NSs-based plasmonic colorimetric sensing, UV-vis spectra of 65.0 μM CC-mediated reduction of Ag$^+$ on the Au NSs at different reaction time were exhibited in Figures S1 and S2, which showed that the blue-shift of the absorption maximum tended to level off within several minutes. These results fully proved the feasibility of the Au NSs-based plasmonic colorimetric sensing for CC detection.
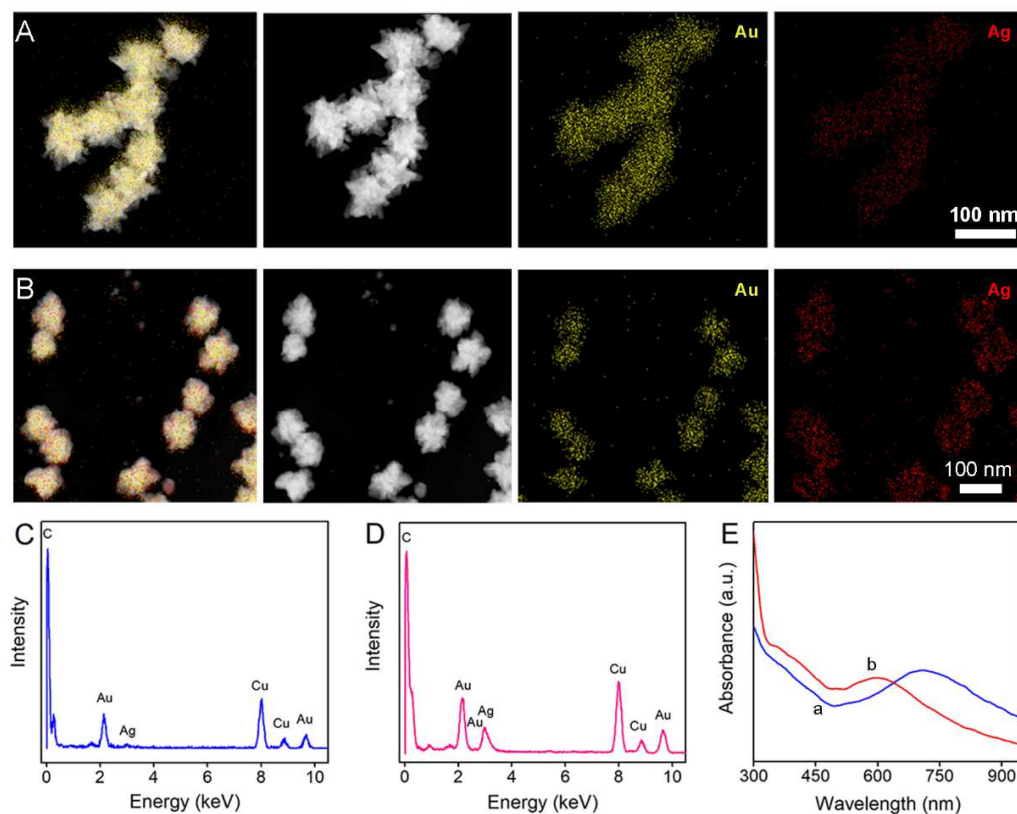

Figure 2. STEM-EDS elemental mapping images of (**A**) 14.0 μM and (**B**) 40.0 μM CC-mediated reduction of Ag$^+$ on the Au NSs. EDS spectrum of (**C**) 14.0 μM and (**D**) 40.0 μM CC-mediated reduction of Ag$^+$ on the Au NSs. (E) UV-vis absorption spectra of (**a**) 14.0 μM and (**b**) 65.0 μM CC-mediated reduction of Ag$^+$ on the Au NSs.

3.3. Mechanism of the Proposed Chemical Sensor

The chemical reaction mechanism was shown in Figure 3. The strong reducing agent CC was easy to reduce Ag$^+$ in alkaline solution to form Ag nanocrystals. When CC is present at lower concentrations, the short supply of reducing agent dictates the slow crystal growths. This facilitates the growth of homogeneous Ag coating on the Au NSs as seeding sites, which yields a blue-shift in the LSPR of the chemical sensor. However, when the concentration of CC is high, the abundant reducing agent favors the nucleation of nanocrystal rather than epitaxial growth, and free-standing Ag nanocrystals are obtained. At this time, the unstable *o*-quinone generated by the oxidation of CC formed a hydrosoluble complex with Au, which manipulated the pink solution [43]. When the CC concentration was higher, the monodisperse Ag nanocrystals gradually grew, and the color of the solution gradually turned yellow.
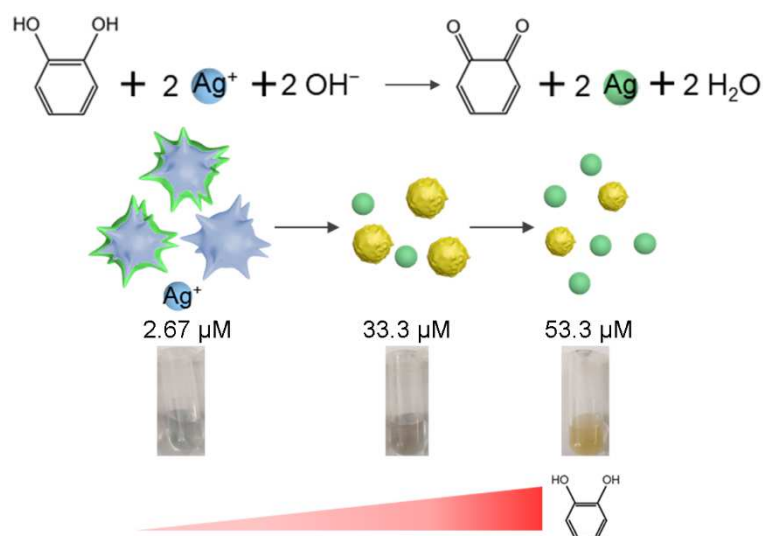
Figure 3. The mechanism of LSPR-based chemical sensor in CC-mediated plasmonic effect on the Au NSs.

3.4. Analytical Performance Evaluation of the Sensor

Encouraged by the sensitive feasibility, the analytical capability of the chemical sensor for different concentrations of CC was investigated. In the presence of Ag$^+$, the absorption peak presented a gradual blue-shift from 818 nm to 548 nm as the concentration of CC varied from 3.33 nM to 107 μM, reflecting the variation of the plasmonic effect of Au NSs (Figure 4A). Noble metal nanomaterials, such as Au, Ag, platinum, and palladium, have strong LSPR effects. By further tuning the size and shape, the plasmon resonance peaks of these materials could be extended into the NIR region. The results of TEM and STEM-EDS images indicated that the reduced Ag nanocrystals gradually covered the surface of the Au NSs, and the sharp arms of Au NSs gradually smoothed as the CC concentration increased, which yielded a blue-shift in the plasma effect of the Au NSs. As shown in Figure 4B, a non-linear relationship between the absorption peak and CC concentrations in the range of 3.33 nM to 107 μM was acquired (R^2 = 0.9979). The detection limit was estimated to be 1 nM, which was calculated based on 3s, where s is the relative standard deviation of the test for blank (20 parallel tests). Benefiting from the strengths of the Ag coatings and the shape of the Au NSs, the linear range and detection limit of the sensor were compared and showed a superior quality to most previously reported methods for detecting CC (Table 1). The results indicated that this plasmonic colorimetric sensing strategy based on the target-mediated plasmonic effect has an appreciable detection performance.
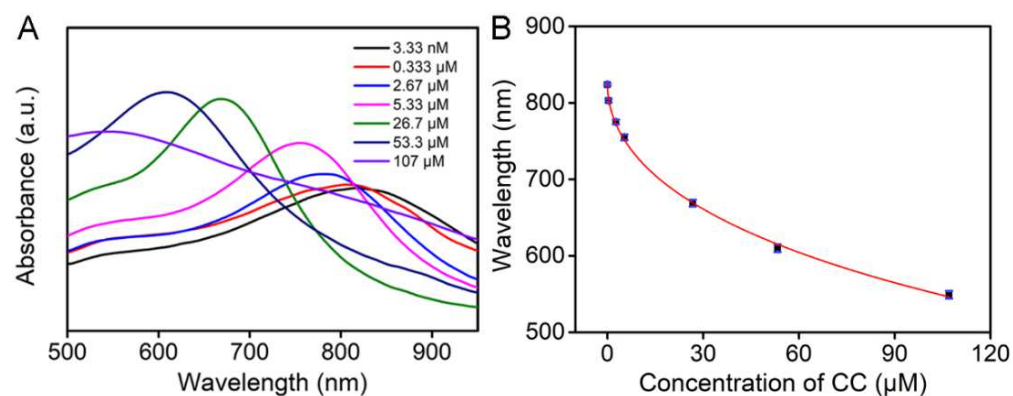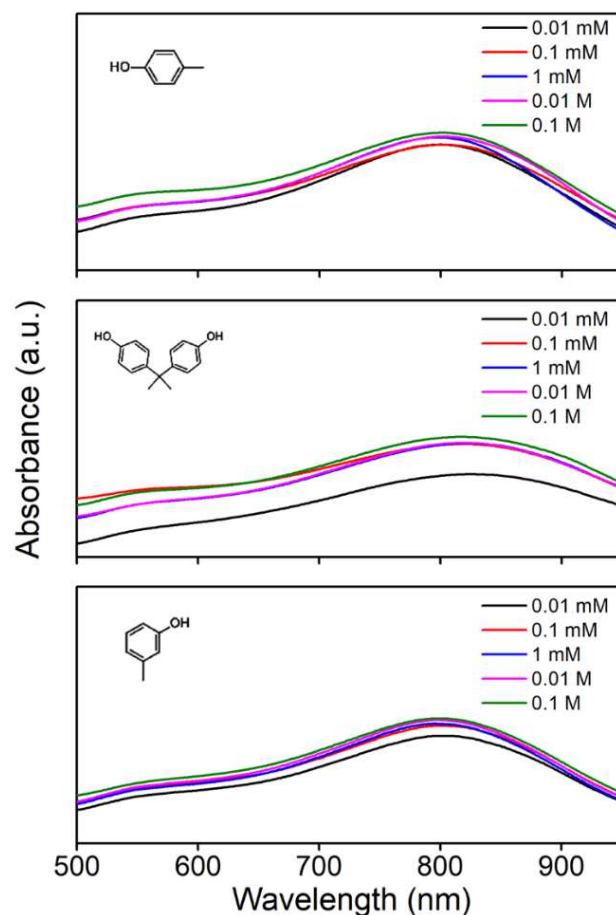

Figure 4. (**A**) UV−vis absorption spectra with different concentrations of CC. (**B**) Standard curve for CC detection based on target-mediated plasmonic colorimetric sensing. The error bars represent the standard deviation of three measurements.

Table 1. Comparison with other reported various methods for CC detection.

Analytical Method	Linear Range	Detection Limit	References
Colorimetry	1 to 1000 µM	0.35 µM	[48]
Fluorescence	0.3 to 40 µM	0.1 µM	[49]
Electrochemistry	0.5 to 190 µM	0.15 µM	[50]
Electrochemistry	10 nM to 22 µM	7.8 nM	[2]
Colorimetry	3.33 nM to 107 µM	1 nM	This Work

The specificity of the chemical sensor was validated by comparing the response toward three other phenolic compounds, namely, *p*-cresol, bisphenol A, and *m*-cresol at different concentration levels. As depicted in Figure 5, unlike CC, the absorption peaks of these compounds did not change significantly with the increase of concentration, indicating that the reduction of Ag^+ was difficult to trigger the plasmonic effect. Further, the oxidation potentials of catechol, *p*-cresol, bisphenol A, and *m*-cresol were about 0.24 V, 0.56 V, 0.88 V, and 0.6 V, respectively [51–53]. The oxidation potential of CC was significantly lower than that of the other three derived structures, revealing that CC is more susceptible to losing electrons and more easily oxidized by this plasmonic colorimetric sensing. It also proved that the sensor has a strong dependence on the chemical properties of the analyte. The stability of this sensor system without CC under various pHs (Figure S3), ionic strengths, and concentrations of other metallic ions (Figure S4) were studied, which revealed that the maximum absorption wavelength has almost no shifts. These results suggest that the developed sensor has encouraging specificity and good stability.

Figure 5. UV−vis absorption spectra of different concentrations of *p*-cresol-, bisphenol A-, and *m*-cresol-mediated reduction of Ag^+ on the Au NSs (from top to bottom).

3.5. Real Sample Detection

To evaluate the practicality of the proposed sensing platform, the standard addition method was employed to determine CC in tap water and industrial wastewater. Among them, the industrial wastewater was filtered through a 0.22 μm membrane and diluted 1000 times. As shown in Figure S5 and Table 2, the recovery values ranged from 96.5 to 108% with RSDs of 4.58–6.08%. The results indicated that the sensor could be applied in the CC analysis of real environmental samples.

Table 2. Recovery results by using as-proposed colorimetric sensor.

Samples	Spiked (μM)	Found (μM)	Recovery (%) $\pm$ SD, *n* = 5
Tap Water	0	Undetected	—
	0.0100	0.0107	107 $\pm$ 5.03
	0.100	0.0980	98.0 $\pm$ 5.36
	10.0	9.65	96.5 $\pm$ 4.58
Industrial Wastewater (1000 Times Diluted)	0	5.01×10^{-3}	—
	0.0100	0.0108	108 $\pm$ 6.08
	0.100	0.103	103 $\pm$ 5.78
	10.0	10.1	101 $\pm$ 5.69

4. Conclusions

In summary, an ultrasensitive plasmonic colorimetric method with wide-range detection of CC was successfully explored based on the target-mediated plasmonic effect, and Au NSs featuring the shape of sea urchins with NIR absorption were synthesized. CC could reduce Ag^+ to form a Ag coating on the surface of Au NSs, which yielded a blue-shift in the LSPR of Au NSs. With the gradual increase in CC concentration, the Ag nanocrystals gradually became free-standing and nucleated to grow, and the degree of blue-shift was greater. The design of this strategy significantly expands the detection range from 3.33 nM to 107 μM and the sensitivity of the colorimetric sensing method, which will pave a new avenue to fabricating an effective analytical platform.

References

1. Wang, H.F.; Wu, Y.Y.; Yan, X.P. Room-Temperature Phosphorescent Discrimination of Catechol from Resorcinol and Hydroquinone Based on Sodium Tripolyphosphate Capped Mn-Doped Zns Quantum Dots. *Anal. Chem.* **2013**, *85*, 1920–1925. [CrossRef] [PubMed]

2. Iftikhar, T.; Aziz, A.; Ashraf, G.; Xu, Y.; Li, G.; Zhang, T.; Asif, M.; Xiao, F.; Liu, H. Engineering MOFs Derived Metal Oxide Nanohybrids: Towards Electrochemical Sensing of Catechol in Tea Samples. *Food Chem.* **2022**, *395*, 133642. [CrossRef] [PubMed]

3. Marrubini, G.; Calleri, E.; Coccini, T.; Castoldi, A.F.; Manzo, L. Direct Analysis of Phenol, Catechol and Hydroquinone in Human Urine by Coupled-Column HPLC with Fluorimetric Detection. *Chromatographia* **2005**, *62*, 25–31. [CrossRef]

4. Liu, C.; Hu, J.; Biswas, S.; Zhu, F.; Zhan, J.; Wang, G.; Tung, C.H.; Wang, Y. Surface-Enhanced Raman Scattering of Phenols and Catechols by a Molecular Analogue of Titanium Dioxide. *Anal. Chem.* **2020**, *92*, 5929–5936. [CrossRef]

5. Piña, S.; Candia-Onfray, C.; Hassan, N.; Jara-Ulloa, P.; Contreras, D.; Salazar, R. Glassy Carbon Electrode Modified with C/Au Nanostructured Materials for Simultaneous Determination of Hydroquinone and Catechol in Water Matrices. *Chemosensors* **2021**, *9*, 88. [CrossRef]

6. de Sá, A.C.; Barbosa, S.C.; Raymundo-Pereira, P.A.; Wilson, D.; Shimizu, F.M.; Raposo, M.; Oliveira, O.N., Jr. Flexible Carbon Electrodes for Electrochemical Detection of Bisphenol-A, Hydroquinone and Catechol in Water Samples. *Chemosensors* **2020**, *8*, 103.

7. Huang, R.; Liao, D.; Chen, S.; Yu, J.; Jiang, X. A Strategy for Effective Electrochemical Detection of Hydroquinone and Catechol: Decoration of Alkalization-Intercalated Ti₃C₂ with MOF-Derived N-Doped Porous Carbon. *Sens. Actuators B Chem.* **2020**, *320*, 128386. [CrossRef]

8. Ma, Y.; Chen, A.Y.; Huang, Y.Y.; He, X.; Xie, X.F.; He, B.; Yang, J.H.; Wang, X.Y. Off-on fluorescent switching of boron-doped carbon quantum dots for ultrasensitive sensing of catechol and glutathione. *Carbon* **2020**, *162*, 234–244. [CrossRef]

9. Sportelli, M.C.; Izzi, M.; Volpe, A.; Clemente, M.; Picca, R.A.; Ancona, A.; Cioffi, N. Novel Polyethylene Oxide Coatings Implementing Ultra-Stable Laser-Ablated Silver Nanoparticles. *Appl. Surf. Sci.* **2020**, *507*, 145156. [CrossRef]

10. Rodriguez-Lorenzo, L.; de la Rica, R.; Alvarez-Puebla, R.A.; Liz-Marzan, L.M.; Stevens, M.M. Plasmonic Nanosensors with Inverse Sensitivity by Means of Enzyme-Guided Crystal Growth. *Nat. Mater.* **2012**, *11*, 604–607. [CrossRef]

11. Li, Z.; Wang, Z.; Li, J.; Zhu, Q.; Wang, Z.; Dai, Z. Enhancing Photoelectric Response of an Au@Ag/AgI Schottky Contact through Regulation of Localized Surface Plasmon Resonance. *J. Am. Chem. Soc.* **2021**, *143*, 13478–13482. [CrossRef] [PubMed]

12. Yue, L.; Yang, K.; Wei, J.; Xu, M.; Sun, C.; Ding, Y.; Yuan, Z.; Wang, S.; Wang, R. Supramolecular Vesicles Based on Gold Nanorods for Precise Control of Gene Therapy and Deferred Photothermal Therapy. *CCS Chem.* **2022**, *4*, 1745–1757. [CrossRef]

13. Deng, X.; Liang, S.; Cai, X.; Huang, S.; Cheng, Z.; Shi, Y.; Pang, M.; Ma, P.; Lin, J. Yolk–Shell Structured Au Nanostar@Metal–Organic Framework for Synergistic Chemo-Photothermal Therapy in the Second Near-Infrared Window. *Nano Lett.* **2019**, *19*, 6772–6780. [CrossRef]

14. Gao, Y.; Wang, J.; Wang, W.; Zhao, T.; Cui, Y.; Liu, P.; Xu, S.; Luo, X. More Symmetrical "Hot Spots" Ensure Stronger Plasmon-Enhanced Fluorescence: From Au Nanorods to Nanostars. *Anal. Chem.* **2021**, *93*, 2480–2489. [CrossRef] [PubMed]

15. Wang, D.; Wang, H.; Ji, L.; Xu, M.; Bai, B.; Wan, X.; Hou, D.; Qiao, Z.Y.; Wang, H.; Zhang, J. Hybrid Plasmonic Nanodumbbells Engineering for Multi-Intensified Second Near-Infrared Light Induced Photodynamic Therapy. *ACS Nano* **2021**, *15*, 8694–8705. [CrossRef] [PubMed]

16. Garcia-Leis, A.; Torreggiani, A.; Garcia-Ramos, J.V.; Sanchez-Cortes, S. Hollow Au/Ag Nanostars Displaying Broad Plasmonic Resonance and High Surface-Enhanced Raman Sensitivity. *Nanoscale* **2015**, *7*, 13629–13637. [CrossRef]

17. Wang, L.; Patskovsky, S.; Gauthier-Soumis, B.; Meunier, M. Porous Au-Ag Nanoparticles from Galvanic Replacement Applied as Single-Particle SERS Probe for Quantitative Monitoring. *Small* **2022**, *18*, 2105209. [CrossRef]

18. Kołątaj, K.; Krajczewski, J.; Kudelski, A. Plasmonic Nanoparticles for Environmental Analysis. *Environ. Chem. Lett.* **2020**, *18*, 529–542. [CrossRef]

19. He, L.; Liu, Y.; Liu, J.; Xiong, Y.; Zheng, J.; Liu, Y.; Tang, Z. Core-Shell Noble-Metal@Metal-Organic-Framework Nanoparticles with Highly Selective Sensing Property. *Angew. Chem. Int. Ed.* **2013**, *52*, 3741–3745. [CrossRef]

20. Azharuddin, M.; Zhu, G.H.; Das, D.; Ozgur, E.; Uzun, L.; Turner, A.P.F.; Patra, H.K. A Repertoire of Biomedical Applications of Noble Metal Nanoparticles. *Chem. Commun.* **2019**, *55*, 6964–6996. [CrossRef]

21. John, A.; Benny, L.; Cherian, A.R.; Narahari, S.Y.; Varghese, A.; Hegde, G. Electrochemical Sensors Using Conducting Polymer/Noble Metal Nanoparticle Nanocomposites for the Detection of Various Analytes: A Review. *J. Nanostructure Chem.* **2021**, *11*, 1–31. [CrossRef]

22. Gu, Y.; Song, J.; Li, M.-X.; Zhang, T.-T.; Zhao, W.; Xu, J.-J.; Liu, M.; Chen, H.-Y. Ultrasensitive microRNA assay via surface plasmon resonance responses of Au@Ag nanorods etching. *Anal. Chem.* **2017**, *89*, 10585–10591. [CrossRef] [PubMed]

23. Jia, M.; Sha, J.; Li, Z.; Wang, W.; Zhang, H. High Affinity Truncated Aptamers for Ultra-Sensitive Colorimetric Detection of Bisphenol a with Label-Free Aptasensor. *Food Chem.* **2020**, *317*, 126459. [CrossRef]

24. Chang, L.; Besteiro, L.V.; Sun, J.; Santiago, E.Y.; Gray, S.K.; Wang, Z.; Govorov, A.O. Electronic Structure of the Plasmons in Metal Nanocrystals: Fundamental Limitations for the Energy Efficiency of Hot Electron Generation. *ACS Energy Lett.* **2019**, *4*, 2552–2568. [CrossRef]

25. Li, D.; Wieckowska, A.; Willner, I. Optical Analysis of Hg^{2+} Ions by Oligonucleotide-Gold-Nanoparticle Hybrids and DNA-Based Machines. *Angew. Chem. Int. Ed.* **2008**, *47*, 3927–3931. [CrossRef] [PubMed]

26. Zeng, J.; Zhang, Y.; Zeng, T.; Aleisa, R.; Qiu, Z.; Chen, Y.; Huang, J.; Wang, D.; Yan, Z.; Yin, Y. Anisotropic Plasmonic Nanostructures for Colorimetric Sensing. *Nano Today* **2020**, *32*, 100855. [CrossRef]

27. Liu, B.; Zhuang, J.; Wei, G. Recent Advances in the Design of Colorimetric Sensors for Environmental Monitoring. *Environ. Sci.-Nano* **2020**, *7*, 2195–2213. [CrossRef]

28. Soh, J.H.; Chan, H.-M.; Ying, J.Y. Strategies for Developing Sensitive and Specific Nanoparticle-Based Lateral Flow Assays as Point-of-Care Diagnostic Device. *Nano Today* **2020**, *30*, 100831. [CrossRef]

29. Zhang, Z.; Wang, H.; Chen, Z.; Wang, X.; Choo, J.; Chen, L. Plasmonic Colorimetric Sensors Based on Etching and Growth of Noble Metal Nanoparticles: Strategies and Applications. *Biosens. Bioelectron.* **2018**, *114*, 52–65. [CrossRef]

30. Li, J.; Kong, C.; Liu, Q.; Chen, Z. Colorimetric Ultrasensitive Detection of DNA Based on the Intensity of Gold Nanoparticles with Dark-Field Microscopy. *Analyst* **2018**, *143*, 4051–4056. [CrossRef]

31. Choi, J.H.; Lim, J.; Shin, M.; Paek, S.H.; Choi, J.W. CRISPR-Cas12a-Based Nucleic Acid Amplification-Free DNA Biosensor via Au Nanoparticle-Assisted Metal-Enhanced Fluorescence and Colorimetric Analysis. *Nano Lett.* **2021**, *21*, 693–699. [CrossRef] [PubMed]

32. Zhang, Y.; Hao, J.; Xu, X.; Chen, X.; Wang, J. Protein Corona-Triggered Catalytic Inhibition of Insufficient POSS Polymer-Caged Gold Nanoparticles for Sensitive Colorimetric Detection of Metallothioneins. *Anal. Chem.* **2020**, *92*, 2080–2087. [CrossRef] [PubMed]

33. Zhou, H.; Yu, Q.; Wang, H.; Zhu, W.; Liu, J.; Wang, Z. A General Scattering Proximity Immunoassay with the Formation of Dimer of Gold Nanoparticle. *Talanta* **2021**, *233*, 122515. [CrossRef]

34. Liu, X.; He, F.; Zhang, F.; Zhang, Z.; Huang, Z.; Liu, J. Dopamine and Melamine Binding to Gold Nanoparticles Dominates Their Aptamer-Based Label-Free Colorimetric Sensing. *Anal. Chem.* **2020**, *92*, 9370–9378. [CrossRef] [PubMed]

35. Zhi, L.; Zhang, S.; Li, M.; Tu, J.; Lu, X. Achieving Ultrasensitive Point-of-Care Assay for Mercury Ions with a Triple-Mode Strategy Based on the Mercury-Triggered Dual-Enzyme Mimetic Activities of Au/WO_3 Hierarchical Hollow Nanoflowers. *ACS Appl. Mater. Interfaces* **2022**, *14*, 9442–9453. [CrossRef] [PubMed]

36. Yuan, X.; Zhou, B.; Li, M.; Shen, M.; Shi, X. Colorimetric Detection of Cr^{3+} Ions in Aqueous Solution Using Poly(γ-Glutamic Acid)-Stabilized Gold Nanoparticles. *Anal. Methods* **2020**, *12*, 3145–3150. [CrossRef]

37. Yu, Y.; Naik, S.S.; Oh, Y.; Theerthagiri, J.; Lee, S.J.; Choi, M.Y. Lignin-Mediated Green Synthesis of Functionalized Gold Nanoparticles Via Pulsed Laser Technique for Selective Colorimetric Detection of Lead Ions in Aqueous Media. *J. Hazard. Mater.* **2021**, *420*, 126585. [CrossRef]

38. Zhuang, Z.; Zhang, C.; Yu, Z.; Liu, W.; Zhong, Y.; Zhang, J.; Xu, Z. Turn-on Colorimetric Detection of Hydroquinone Based on Au/CuO Nanocomposite Nanozyme. *Mikrochim. Acta* **2022**, *189*, 293. [CrossRef]

39. Choi, H.; Kang, T.; Um, K.; Kim, J.; Lee, K. Reduction of Silver Ions in Gold Nanoparticle Suspension for Detection of Dihydroxy-benzene Isomers. *Colloid. Surf. A* **2014**, *459*, 120–127. [CrossRef]

40. Guo, L.; Xu, Y.; Ferhan, A.R.; Chen, G.; Kim, D.H. Oriented Gold Nanoparticle Aggregation for Colorimetric Sensors with Surprisingly High Analytical Figures of Merit. *J. Am. Chem. Soc.* **2013**, *135*, 12338–12345. [CrossRef]

41. Xianyu, Y.; Lin, Y.; Chen, Q.; Belessiotis-Richards, A.; Stevens, M.M.; Thomas, M.R. Iodide-Mediated Rapid and Sensitive Surface Etching of Gold Nanostars for Biosensing. *Angew. Chem. Int. Ed.* **2021**, *60*, 9891–9896. [CrossRef] [PubMed]

42. Castaño-Guerrero, Y.; Romaguera-Barcelay, Y.; Moreira, F.T.C.; Brito, W.R.; Fortunato, E.; Sales, M.G.F. Poly(Thionine)-Modified Screen-Printed Electrodes for CA 19-9 Detection and Its Properties in Raman Spectroscopy. *Chemosensors* **2022**, *10*, 92. [CrossRef]

43. Cui, X.; Wei, T.; Hao, M.; Qi, Q.; Wang, H.; Dai, Z. Highly Sensitive and Selective Colorimetric Sensor for Thiocyanate Based on Electrochemical Oxidation-Assisted Complexation Reaction with Gold Nanostars Etching. *J. Hazard. Mater.* **2020**, *391*, 122217. [CrossRef] [PubMed]

44. Liu, J.; Lu, Y. Preparation of Aptamer-Linked Gold Nanoparticle Purple Aggregates for Colorimetric Sensing of Analytes. *Nat. Protoc.* **2006**, *1*, 246–252. [CrossRef]

45. Pazos-Perez, N.; Guerrini, L.; Alvarez-Puebla, R.A. Plasmon Tunability of Gold Nanostars at the Tip Apexes. *ACS Omega* **2018**, *3*, 17173–17179. [CrossRef] [PubMed]

46. Siegel, A.L.; Baker, G.A. Bespoke Nanostars: Synthetic Strategies, Tactics, and Uses of Tailored Branched Gold Nanoparticles. *Nanoscale Adv.* **2021**, *3*, 3980–4004. [CrossRef]

47. Shameli, K.; Ahmad, M.B.; Jazayeri, S.D.; Shabanzadeh, P.; Sangpour, P.; Jahangirian, H.; Gharayebi, Y. Investigation of Antibacterial Properties Silver Nanoparticles Prepared via Green Method. *Chem. Cent. J.* **2012**, *6*, 73. [CrossRef]

48. Liu, X.; Yang, J.; Cheng, J.; Xu, Y.; Chen, W.; Li, Y. Facile Preparation of Four-in-One Nanozyme Catalytic Platform and the Application in Selective Detection of Catechol and Hydroquinone. *Sens. Actuator. B Chem.* **2021**, *337*, 129763. [CrossRef]

49. Zhao, X.-E.; Zuo, Y.-N.; Xia, Y.; Sun, J.; Zhu, S.; Xu, G. Multifunctional NH_2-Cu-MOF Based Ratiometric Fluorescence Assay for Discriminating Catechol from Its Isomers. *Sens. Actuator. B Chem.* **2022**, *371*, 132548. [CrossRef]
50. Yin, D.; Liu, J.; Bo, X.; Guo, L. Cobalt-Iron Selenides Embedded in Porous Carbon Nanofibers for Simultaneous Electrochemical Detection of Trace of Hydroquinone, Catechol and Resorcinol. *Anal. Chim. Acta* **2020**, *1093*, 35–42. [CrossRef]
51. Lounasvuori, M.M.; Kelly, D.; Foord, J.S. Carbon Black as Low-Cost Alternative for Electrochemical Sensing of Phenolic Compounds. *Carbon* **2018**, *129*, 252–257. [CrossRef]
52. Ye, Z.; Wang, Q.; Qiao, J.; Ye, B.; Li, G. Simultaneous Detection of Bisphenol A and Bisphenol S with High Sensitivity Based on A New Electrochemical Sensor. *J. Electroanal. Chem.* **2019**, *854*, 113541. [CrossRef]
53. González-Costas, J.M.; Gómez-Fernández, S.; García, J.; González-Romero, E. Screen-Printed Electrodes-Based Technology: Environmental Application to Real Time Monitoring of Phenolic Degradation by Phytoremediation with Horseradish Roots. *Sci. Total Environ.* **2020**, *744*, 140782. [CrossRef] [PubMed]